Batteries & Supercaps

Research Article
doi.org/10.1002/batt.202300103

Chemistry Europe
European Chemical Societies Publishing

www.batteries-supercaps.org

Special Collection

Achieving Enhanced Electrochemical Performance for Cobalt-Free Layered Cathode Material by Aluminum Doping

Mingyuan Ma,[a] Dan Yang,[a] Yongsheng Ji,[a] Long Qie,[b] Zhikang Liu,*[a] and Yunhui Huang*[a, b]

We introduce a facile strategy to greatly improve the electrochemical reversibility of cobalt-free cathode material by doping trace quantity of aluminum (Al) in $LiNi_{0.65}Mn_{0.35}O_2$. X-ray diffraction and X-ray photoelectron spectroscopy results reveal that Al doping reduces the cation disorder consequently and hence increases structural stability. Electrochemical measurements show that rate capability and cycling stability are remarkably enhanced by Al doping. Al-doped $LiNi_{0.65}Mn_{0.35}O_2$ exhibits the optimized electrochemical performance with a capacity retention of 94.2% after 200 cycles at 2 C in voltage range of 2.75–4.2 V in cylindrical full cell, demonstrating that Al-doped cathode exhibits enhanced cyclability, reduced polarization and high-rate capability during charge/discharge process. Moreover, the full cell shows good low-temperature performance with more than 70% capacity retention at −20 °C. The improved performances can be ascribed to the enhanced stability in layered structure of the Co-free material by the support of doped Al ions.

Introduction

Lithium-ion batteries (LIBs) are widely used as the power sources for portable electronic devices, electric vehicles (EVs), and large-scale storage application.[1–6] With the urged demand of high-energy-density LIBs, much effort has been devoted to exploring the novel cathode materials. Among various cathode materials, nickel-based layered oxide cathodes possess high capacity and working voltage, and hence are regarded as highly promising materials.[7–10] Some typical Ni-based materials like $LiNi_{0.5}Co_{0.2}Mn_{0.3}O_2$ and $LiNi_{0.8}Co_{0.15}Al_{0.05}O_2$ have already been widely commercialized in the EVs market. To further boost the energy density of state-of-the-art LIBs above 300 Wh kg^{-1}, a higher nickel content in $LiNi_{1-x}M_xO_2$ ($1-x>0.8$, M=Co, Al, Mn, etc.) are pursued.[11–14] Under such a background, many companies are eager to realize the commercialization of cobalt-free cathode materials so as to get rid of the dependence on cobalt resource and effectively reduce the cost of power batteries. Therefore, it is very important to develop cathode materials with low cobalt content or even no cobalt.

Typically, $LiNi_{0.5}Mn_{0.5}O_2$ (LNM) has been extensively studied since first reported by Ohzuku and his coworkers.[13] However, the major shortcoming of such transition metal (TM) layered oxides containing Mn and Ni is high-degree Ni^{2+}/Li^+ cation disorder. Due to the similar ionic radius of Li^+ and Ni^{2+} (0.76 and 0.69 Å, respectively), Ni^{2+} ions typically migrate to 3a sites in the Li layer while Li^+ ions migrate to 3b sites in the transition metal (TM) layer,[15–18] which affects the rate capability and structural stability of the LNM material. Therefore, it is necessary to reduce the Ni^{2+}/Li^+ disorder degree.

In this work, we propose an effective strategy to partly replace M (M=Mn, Ni) in LNM by aluminum doping. Compared with the undoped counterpart, the introduction of Al reduces the cation disorder and achieves high-rate discharge capability, so that this material can meet the requirement of commercial application.

Results and Discussion

XRD patterns of as-prepared LNM cathodes are presented in Figure 1. For LNMA, the diffraction peaks correspond to a layered hexagonal α-$NaFeO_2$ structure with $R\bar{3}m$ space group, indicating that Al-incorporation does not alter the crystal structure of LNM. Furthermore, the observed splitting of (006)/(102) and (018)/(110) peaks indicates the presence of well-developed layered structure.[21]

Furthermore, Rietveld refinement was utilized to study the influence of Al incorporation on structure. The results are presented in Figure 1(c and d) and Table 1. R_{wp} values of LNM and LNMA are lower than 4%, indicative of the reliability of refinement.[16] The Li^+/Ni^{2+} disorder degrees in LNM and LNMA are 6.12% and 4.80%, respectively, showing that the Li/Ni disorder is successfully alleviated by Al incorporation. It can be

[a] Dr. M. Ma, Dr. D. Yang, Dr. Y. Ji, Dr. Z. Liu, Prof. Y. Huang
Institute of New Energy Vehicles
School of Materials Science and Engineering
Tongji University
Shanghai 201804 (P.R. China)
E-mail: zkliu0904@tongji.edu.cn
[b] Prof. L. Qie, Prof. Y. Huang
State Key Laboratory of Material Processing and Die & Mould Technology
School of Materials Science and Engineering
Huazhong University of Science and Technology
Wuhan 430074 (P.R. China)
E-mail: huangyh@hust.edu.cn

Supporting information for this article is available on the WWW under https://doi.org/10.1002/batt.202300103

Special Collection An invited contribution to a Special Collection on Fast Charging Batteries

Research Article
doi.org/10.1002/batt.202300103
Chemistry Europe
European Chemical Societies Publishing

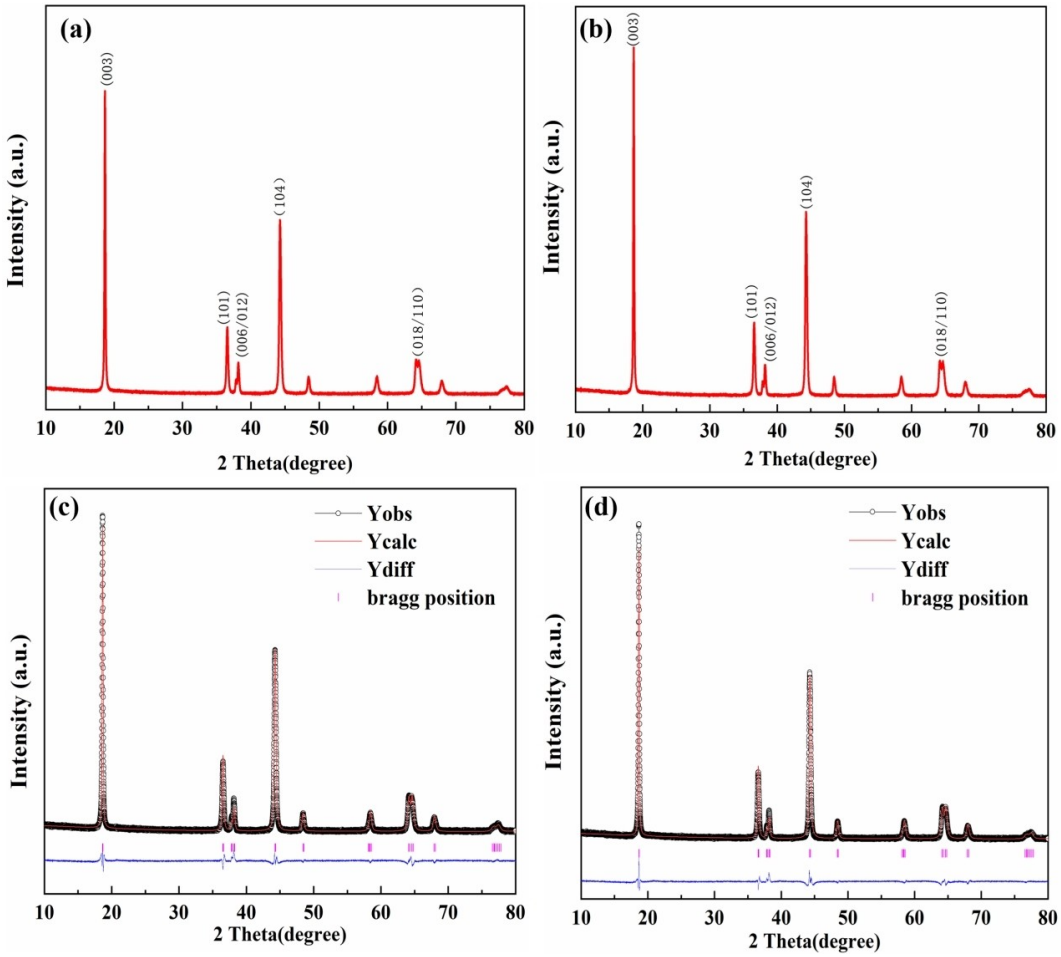

Figure 1. XRD patterns of as-prepared materials. a) LNM, b) LNMA, c) Refinement-LNM, and d) Refinement-LNMA.

Table 1. The structural parameters from Rietveld analysis.

Sample	*a*	*b*	*c*	*c*/*a*	Ni/Li	R_w (%)	R_p (%)	CH*2
LNM	2.882 (0.1)	2.882 (0.1)	14.27 (1)	4.9503	6.12%	2.38	1.65	2.921
LNMA	2.882 (0.1)	2.882 (0.1)	14.271 (1)	4.9504	4.80%	2.39	1.68	3.008

found that the LNMA exhibits lower Li/Ni disorder, which is attributed to the occupation of transition metal sites by Al without forming any impurity phase. Moreover, Al introduction mitigates the change from Ni^{3+} to Ni^{2+} due to the formation of Li^+ vacancy and strong Al–O bond.[22] The calculated lattice parameters are listed in Table 1. Parameter "*a*" represents the distance between the transition metal layers, while parameter "*c*" stands for the sum of slab thickness and inter-slab space thickness. The *c*/*a* value of LNMA is higher than that of LNM, which means that the lattice of LNMA be inclined to grow along the c-axis, which Lowers energy barrier of Li^+ diffusion in the lithium layer, and hence accelerates the diffusion of Li^+ and improves the rate performance.[23]

XPS spectra were carried out to examine chemical environments and relative valent states of transition metal cations for cobalt-free layered LNM and LNMA. Figure 2 unravels high-resolution Ni 2p XPS characteristic peaks of different powders coupled with fitting patterns. The main peak of Ni $2p_{1/2}$ is located at 872.4 eV, while satellite peak of Ni $2p_{1/2}$ at 879.4 eV, and the satellite peak at 860.6 eV are regarded as Ni $2p_{3/2}$. According to the fitted XPS data, both Ni $2p_{1/2}$ and Ni $2p_{3/2}$ have two splitting peaks corresponding to Ni^{2+} and Ni^{3+}, respectively. The fitting results of Ni $2p_{3/2}$ display two binding energy peaks of Ni^{2+} and Ni^{3+} at 855.6 and 854.2 eV, while Ni $2p_{1/2}$ peaks of Ni^{2+} and Ni^{3+} at 873.6 and 871.7 eV, respectively. These peak positions are consistent with previous studies.[16] The Ni^{2+} ratio in LNM is 65.9%, which is higher than that in LNMA (60.6%). By contrast, the content of Ni^{2+} in cobalt-free LNMA is lower, which alleviates the cation Li^+/Ni^{2+} disorder, thus improving the electrochemical performance.

Scanning electron microscopy (SEM) was used to observe the morphologies of LNM and LNMA. These two samples show irregular secondary particles composed of flaky primary particles (Figure 3a, b). And a uniform secondary particle size about 3 μm can be observed. Besides, the size of this material was also analyzed using a laser particle size analyzer, as the results presented in Supporting Information Figure S1. Furthermore, the layered structures of LNM and LNMA are further

Research Article
doi.org/10.1002/batt.202300103
Chemistry Europe
European Chemical Societies Publishing

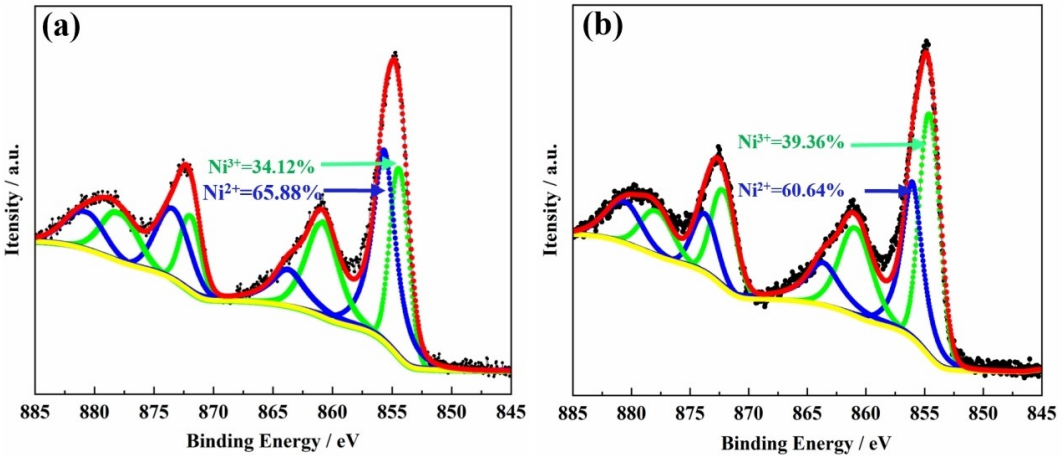

Figure 2. XPS spectra of Ni 2p of a) LNM, and b) LNMA cobalt-free cathode.

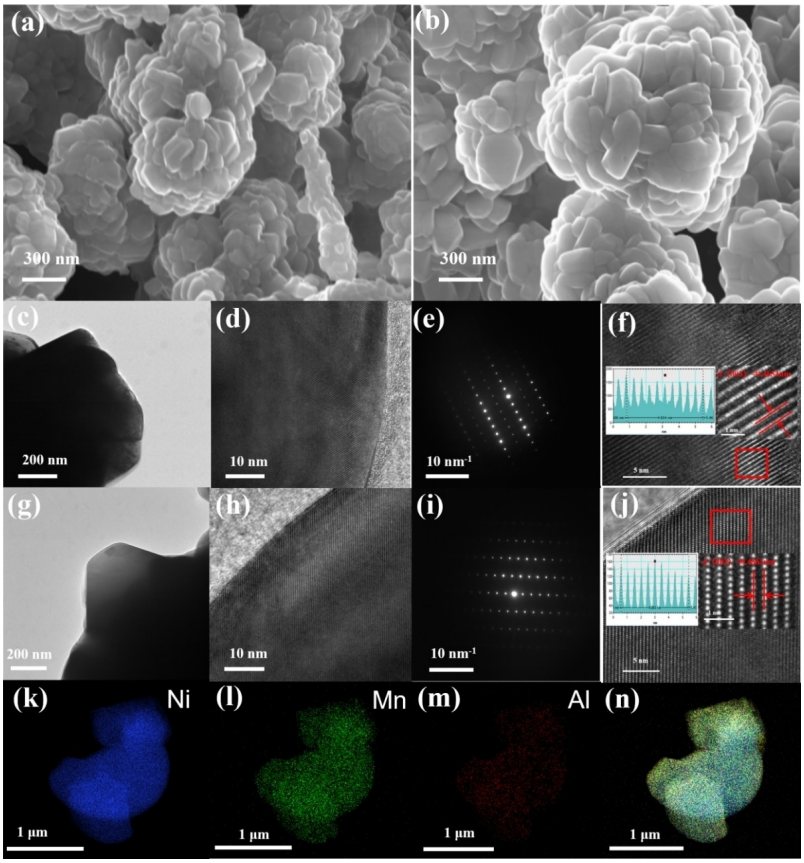

Figure 3. SEM images of as-prepared materials. a) LNM, b) LNMA. HRTEM and the corresponding line intensity profile images for c–f) pristine LNM and g–j) LNMA materials. K–n) EDS elemental mapping of LNMA.

identified by high-resolution transmission electron microscopy (HRTEM). As seen from the HRTEM images, the LNM exhibits obvious layered structure with clear and uniform lattice spacing of 0.4654 nm (Figure 3c–f), corresponding to the $R\bar{3}m$ structure (003) crystal planes, which can be further identified by selected area electron diffraction. In comparison, the lattice spacing of plane (003) for LNMA increases to 0.4863 nm after Al-doping, corresponding to the selected area electron diffraction results, which is favor for Li^+ diffusion (Figure 3g–j). Besides, the energy dispersive spectroscopy (EDS) mappings of LNMA indicate the uniform dispersion of Ni, Mn, O and Al in the particle.

The presence of Al as a counterbalancing cation for Mn to suppress Li/Ni disorder is believed to be critical for LNMA in the absence of Co. Importantly, the rate capability is a key performance for LNMA to compete against $LiNi_xCo_yMn_{(1-x-y)}O_2$. To compare electrochemical performances of LNM and LNMA,

a series of galvanostatic tests and full-cell tests were performed. Figure 4(a and b) shows initial charge-discharge profiles of LNM and LNMA at 0.1 C between 2.75 and 4.25 V. All the charge/discharge curves display similar shape, indicating that no extra electrochemical reaction is caused by the doping. With the doping of Al, the initial discharge capacity basically does not change between LNM (164.4 mAh g^{-1}) and LNMA (164.0 mAh g^{-1}). By further studying the effect of different doping amounts and sintering temperature on properties, it can be found that the best performance is achieved when the doping amount of aluminum is at 1500 ppm and the temperature is at 850 °C (Figure S2 and Table S1, Figure S3 and Table S3). Meanwhile, LNM and LNMA exhibit high and similar coulombic efficiency of 93.7% and 93.9%, respectively. This observation indicates that LNMA has better reversibility despite of the presence of inactive Al, attributing to additional Li^+ de/intercalation sites that reduce the irreversible specific capacity loss. Figure 4(d) shows full-cell rate capacities of LNMA. Even when the current rate reaches 5 C, the discharge capacity of LNMA is unchanged basically. Beside, Figure 4(c) shows that the full-cell capacity retention is more than 70% at −20 °C under the condition of 1 C rate discharge. In order to make the lithium-ion battery work normally at −20 °C, it is very necessary to test the low-temperature discharge performance. Al doping reduces the Ni^{2+}/Li^+ cation disorder, and is also conducive to the reduction of electrochemical impedance. Therefore, it is obvious that doping can improve the rate capability of pristine LNM effectively.

Figure 5(a) displays coin-cell cycling performance of LNM and LNMA. After being activated at 0.1 C for the initial three cycles, both LNM and LNMA were cycled at 0.5 C for 100 cycles. As observed, LNM and LNMA deliver the capacity retention of 78.2% and 86.4%, respectively. It is superior to the data currently reported in the literatures (Table S2). LNMA shows higher capacity retention, indicating that doping strategy can effectively enhance cycling stability, thus leading to improved cycling performance. To assess the commercial viability of the Co-free LNMA cathode, the cathode was tested in a cylindrical-type full cell using a graphite anode to evaluate its long-term cycling stability. The full cells were tested at a voltage up to 4.2 V (vs. graphite) at a current density of 2.0 C (4400 mA g^{-1}). As shown in Figure 5(b), the Co-free LNMA maintains 94.2% of its initial capacity after 200 cycles, which is able to meet the life requirement of the market. The long-term cycling stability and the discharge rate stability further demonstrate that the proposed LNMA is a promising Co-free cathode material for practical application under normal charging cut-off voltage conditions (2.75–4.2 V).

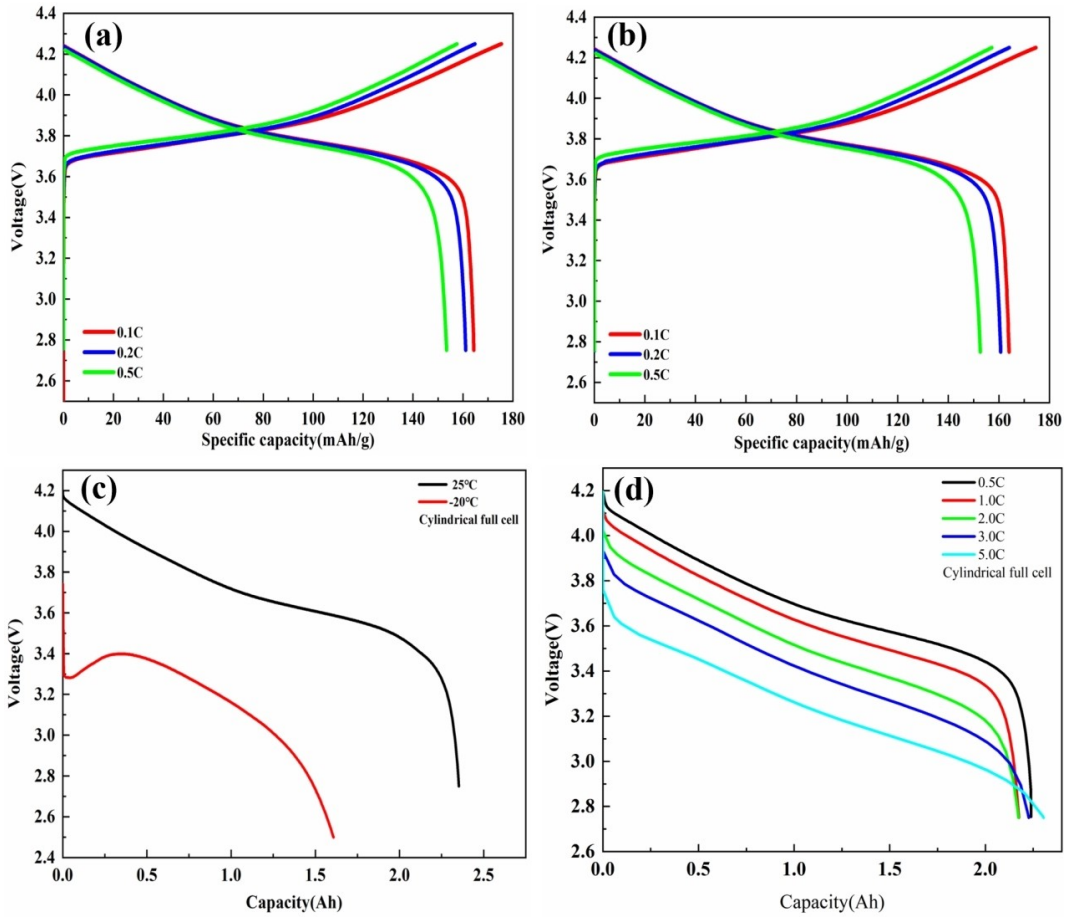

Figure 4. Corresponding rate charge/discharge curves of a) LNM, b) LNMA, c) Corresponding LNMA discharge capacity curves of at different temperature. d) Corresponding LNMA cathodes discharge capacity curves at various current densities.

Research Article
doi.org/10.1002/batt.202300103
Chemistry Europe
European Chemical Societies Publishing

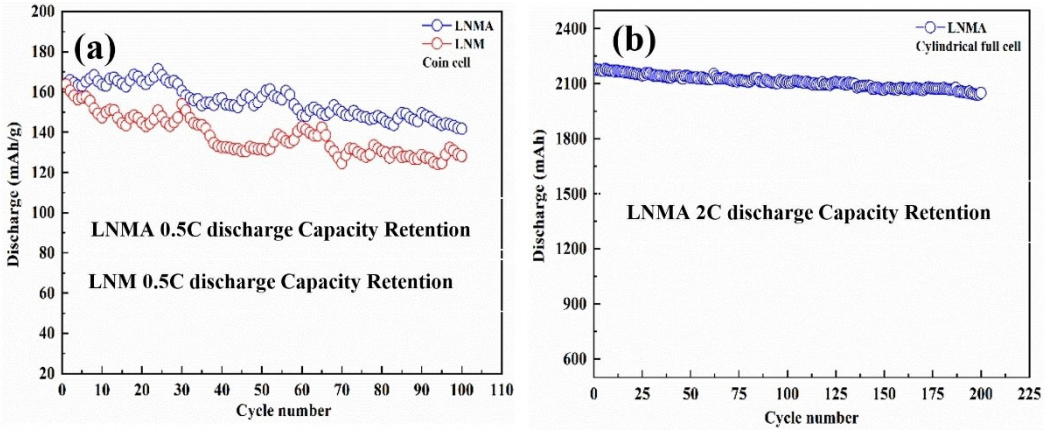

Figure 5. Electrochemical performances of cathodes in the voltage range of 2.75–4.25 V and 2.75–4.20 V. a) coin cell cycling stability and b) cylindrical full cell cycling stability.

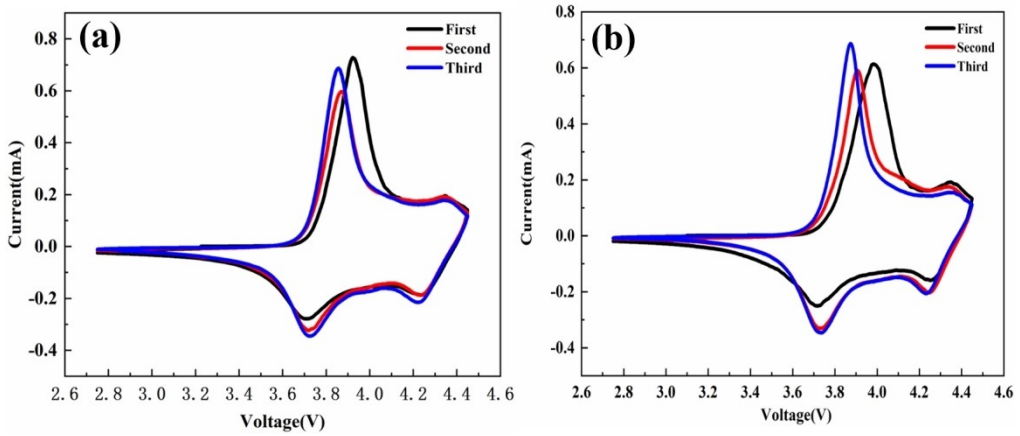

Figure 6. CV curves of a) LNM and b) LNMA cathodes. The CV curves were measured in the voltage range of 2.75–4.45 V (vs. Li/Li^+) at the scan rate of 0.5 mV/s.

In order to understand electrochemical lithium storage behaviors in detail, cyclic voltammogram (CV) curves of LNM and LNMA in the initial three cycles were attained at a scanning rate of 0.5 $mV\,s^{-1}$ in a voltage range of 2.75–4.45 V, as shown in Figure 6. The oxidation peak at approximately 3.9 V and the reduction peak at about 3.7 V correspond to the Ni^{4+}/Ni^{2+} redox couple. Alien ion introduction can not only stabilize the material structure, but also impact the operating voltage of electrode materials. For both LNM and LNMA, the oxidation peak (V_O) shifts to a lower potential after the first cycle. The unchanged reduction peak position implies that the material has excellent reversibility.[24] Further analysis of the electric potential (ΔV) between Redox peaks can well understand the effect on the polarization behavior. Table 2 clearly shows that LNM displays the larger polarization after three cycles. Compared with LNM, Al substitution for both Ni and Mn exhibits smaller polarization, while the LNMA cathode shows the smaller polarization. The reduction of polarization improves electrochemical performance. Al substitution at Ni or Mn sites is beneficial for improving the reversibility of free-cobalt layered cathodes. On the other hand, the operating voltage difference can also be concluded according to Figure 6 and Table 2. When discharging, the Co-free LNMA cathode shows the highest discharge voltage of about 3.74 V, which is higher than LNM (3.72 V). The results demonstrate that Al substitution for Mn and Ni can raise the discharge voltage of Co-free layered cathode materials. Raising the discharge voltage is beneficial to improve the energy density of LIBs, which is quite essential for powering electric vehicles. The changes in the operating voltage and polarization effect give rise to a comprehensive insight into understanding the effect on electrochemical process of Co-free layered cathodes materials.

Table 2. The parameters from CV curves.

LNM				LNMA		
	V_O	V_R	δ	V_O	V_R	δ
first	3.9222	3.7125	0.2097	3.9828	3.7143	0.2685
second	3.8701	3.7194	0.1507	3.9084	3.7349	0.1735
third	3.8559	3.7222	0.1337	3.8757	3.7432	0.1325

To further examine the difference between LNM and LNMA electrodes, electrochemical impedance spectroscopy (EIS) tests were also performed to investigate the Li^+ diffusion coefficient.

Research Article
doi.org/10.1002/batt.202300103
Chemistry Europe
European Chemical Societies Publishing

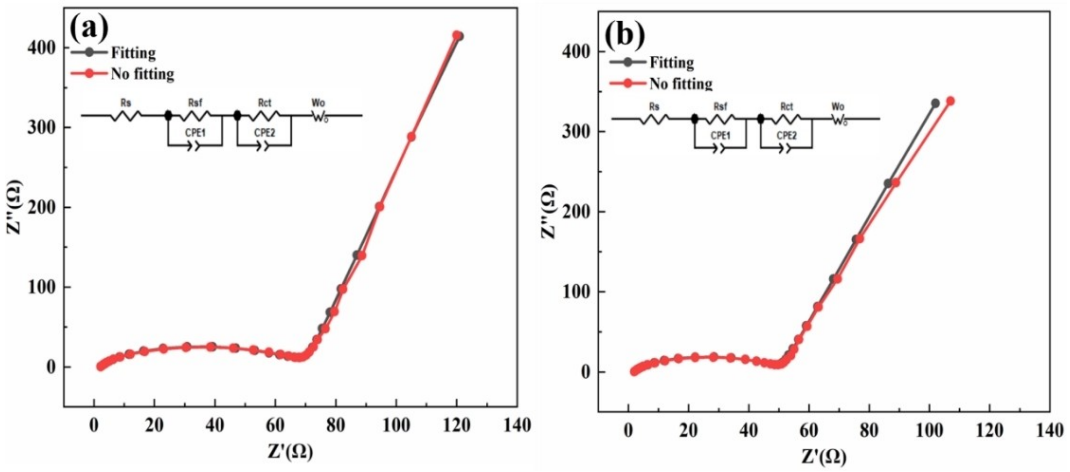

Figure 7. a) Nyquist plot of the pristine LNM electrode with the fitted curve. b) Nyquist plot of LNMA electrode with a fitted curve.

The EIS spectra of LNM and LNMA are shown in Figure 7, and the specific parameters are shown in Table 3. The intercept at high frequency corresponds to the electrolyte resistance (R_s), The semicircle in high frequency stands for the charge transfer at the interface between electrolyte and electrode (R_{ct}). The straight line in the low frequency region represents the diffusion rate of lithium ions in cathode materials (W_o).[25–27] The R_{ct} values of LNM and LNMA are 58.58 and 43.05 Ω, respectively. The LNMA cathode evidently exhibits a lower impedance than that of LNM, indicating an enhanced electron and ion transport. Also, the LNMA electrode exhibits smaller R_s and W_o values than those of the LNM electrode. The smaller impedance of LNMA can be attributed to the small particle size and larger lattice space, which dramatically reduces the Li^+ diffusion distance, enabling a fast transport rate.

Conclusions

We have synthesized Al-incorporated Co-free LNMA layered cathode materials using a simple coprecipitation and sintering method, and systematically investigated the physicochemical properties. The obtained LNMA cathode exhibits higher rate capability and better cycling stability compared with LNM. The enhanced stability is mainly attributed to the improved chemical stability. On the other hand, our result breaks the saying that the absence of Co deteriorates the rate capability of the LNM cathode, particularly at low temperature. The long-term cycling stability of the LNMA cathode is also verified in a full cell, demonstrating that LNMA is a promising Co-free cathode for commercial application. This work not only provides a fundamental insight into redefining the Ni-rich Co-free cathode material, but also demonstrates the possibility for developing Co-free Ni-rich layered cathode materials for high-voltage and high-rate applications.

Table 3. Resistance differences analysis according to EIS plots.

LNM			LNMA		
R_S	R_{ct}	W_O	R_S	R_{ct}	W_O
2.035	58.58	27.98	1.771	43.05	17.02
0.98%	1.63%	13.81%	1.39%	2.91%	26.97%

Experimental Section

The co-precipitation method was used to synthesize $LiNi_{0.65}Mn_{0.35}O_2$. Firstly, 0.35 mmol $MnSO_4$ (Dalian Ruiyuan Power Co., Ltd) and 0.65 mmol $NiSO_4 \cdot 6H_2O$ (Jinchuan Group Co., Ltd) were dissolved into 40 mL deionized water, while 20 mmol $NH_3 \cdot H_2O$ (Taixing Sucheng Chemical Co., Ltd) was dissolved into another 30 mL deionized water. Secondly, the ammonia solution was dropwise added into the metal-salt solution with vigorous stirring for 72 h. The obtained coprecipitation was filtered, washed, and dried at 80 °C to get $Ni_{0.65}Mn_{0.35}(OH)_2$. Finally, the obtained $Ni_{0.65}Mn_{0.35}(OH)_2$ precursor was mixed with $LiOH \cdot H_2O$ (molar ratio of Li/(Ni + Co + Mn) = 1.08), and preliminarily calcinated at 450 °C for 5 h and then sintered at 850 °C for 12 h under flowing O_2 gas. The obtained $LiNi_{0.65}Mn_{0.35}O_2$ was denoted as LNM.

In order to obtain the Al-incorporated $LiNi_{0.65}Mn_{0.35}O_2$, the $Ni_{0.65}Mn_{0.35}(OH)_2$ precursor was mixed with $LiOH \cdot H_2O$ (molar ratio of Li/(Ni + Co + Mn) = 1.08) and nanometer Al_2O_3 with different amounts (20–30 nm, Innochem (Beijing) Technology Co., Ltd) for 30 min at a speed of 200 r/min in high speed mixing machine. Then the product preliminarily calcinated at 450 °C for 5 h and further sintered at 850 °C for 12 h under flowing O_2 gas. The obtained $LiNi_{0.65}Mn_{0.35}Al_xO_2$ was denoted as LNMA.

X-ray diffraction (XRD, Bruker AXS 3000) with Cu–Kα radiation was used to confirm the structure and phase of the materials. The elemental mapping and surface morphology were examined by scanning electron microscopy (SEM, ZEISS, Sigma-300) at an accelerating voltage of 20 kV and transmission electron microscopy (TEM, Talos, F-200X). X-ray photoelectron spectroscopy (XPS, Thermo Scientific, K-Alpha+) was used to analyze the chemical condition of major elements on the surface of materials.

The cathodes were prepared by casting a slurry containing LNM or LNMA, acetylene black, and poly (vinylidene fluoride) binder with a weight ratio of 90:5:5 onto Al current collector, then were dried at 120 °C for 12 h at vacuum overnight and punched into disks with the diameter of 1.26 cm before use. The active material loading

amount was about 5 mg cm^{-2}. The R2032 coin-type cells consisting of the as-prepared cathode, the anode (metallic lithium foil), the PE separator, and the electrolyte (1.0 M $LiPF_6$ in ethyl carbonate: ethyl methyl carbonate (EC:EMC) = 4:6) were assembled in an argon filled glovebox with both the water and oxygen content less than 0.1 ppm. The electrochemical performance of the assembled cells was evaluated on the BTS cell testing instrument (NEWARE Electronic Co., Ltd.) at various rates (1 C = 250 mA g^{-1}) in the voltage range of 2.75–4.25 V. Electrochemical impedance spectroscopy (EIS) of the cells was measured under the charged state of 4.45 V at the frequency from 10^5 to 10^{-2} Hz with potential perturbation amplitude of 10 mV using the electrochemical workstation of Bio-Logic electrochemistry workstation.

Acknowledgements

This work was supported by the National Natural Science Foundation of China (Grant No. 5202780089).

Conflict of Interests

The authors declare no conflict of interest.

Data Availability Statement

The data that support the findings of this study are available from the corresponding author upon reasonable request.

Keywords: aluminum-doping · cobalt-free cathode · full cell · low-temperature performance · rate capability

[1] J. B. Goodenough, K.-S. Park, *J. Am. Chem. Soc.* **2013**, *135*, 1167–1176.
[2] W. Li, E. M. Erickson, A. Manthiram, *Nat. Energy* **2020**, *5*, 26.
[3] J.-M. Tarascon, M. Armand, *Nature* **2001**, *414*, 359.
[4] K. Ariyoshi, T. Ichikawa, T. Ohzuku, *J. Phys. Chem. Solids* **2008**, *69*, 1238–1241.
[5] J. B. Goodenough, *Nat. Electron.* **2018**, *1*, 204.
[6] C. Hong, Q. Leng, J. Zhu, S. Zheng, H. He, Y. Li, R. Liu, J. Wan, Y. Yang, *J. Mater. Chem. A* **2020**, *8*, 8540.
[7] T.-H. Kim, J.-S. Park, S. K. Chang, S. Choi, J. H. Ryu, H.-K. Song, *Adv. Energy Mater.* **2012**, *2*, 860.
[8] Y. Kim, W. M. Seong, A. Manthiram, *Energy Storage Mater.* **2021**, *34*, 250.
[9] S.-W. Lee, M.-S. Kim, J. H. Jeong, D.-H. Kim, K. Y. Chung, K. C. Roh, K.-B. Kim, *J. Power Sources* **2017**, *360*, 206–214.
[10] A. Manthiram, *Nat. Commun.* **2020**, *11*, 1550–1558.
[11] J. Kim, H. Cha, H. Lee, P. Oh, J. Cho, *Batteries & Supercaps* **2020**, *3*, 309–322.
[12] T. Liu, L. Yu, J. Liu, J. Lu, X. Bi, A. Dai, M. Li, M. Li, Z. Hu, L. Ma, D. Luo, J. Zheng, T. Wu, Y. Ren, J. Wen, F. Pan, K. Amine, *Nat. Energy* **2021**, *6*, 277–286.
[13] Y. Makimura, T. Ohzuku, *J. Power Sources* **2003**, *119*, 156–160.
[14] H. Maleki Kheimeh Sari, X. Li, *Adv. Energy Mater.* **2019**, *9*, 1901597.
[15] R. Torchio, C. Marini, Y. O. Kvashnin, I. Kantor, O. Mathon, G. Garbarino, C. Meneghini, S. Anzellini, F. Occelli, P. Bruno, A. Dewaele, S. Pascarelli, *Phys. Rev. B* **2016**, *94*, 024429.
[16] L. Wang, G. Liu, X. Ding, C. Zhan, X. Wang, *ACS Appl. Mater. Interfaces.* **2019**, *11*, 33901–33912.
[17] T. Weigel, F. Schipper, E. M. Erickson, F. A. Susai, B. Markovsky, D. Aurbach, *ACS Energy Lett.* **2019**, *4*, 508–516.
[18] J. Xie, Y. Lu, *Nat. Commun.* **2020**, *11*, 2499.
[19] J. Zheng, S. Myeong, W. Cho, P. Yan, J. Xiao, C. Wang, J. Cho, J. Zhang, *Adv. Energy Mater.* **2016**, *7*, 1601284.
[20] J. Zheng, Y. Ye, T. Liu, Y. Xiao, C. Wang, F. Wang, F. Pan, *Acc. Chem. Res.* **2019**, *52*, 2201–2209.
[21] X. Chen, X. Jia, Y. Qu, D. Li, D. Chen, Y. Chen, *New J. Chem.* **2018**, *42*, 5868–5874.
[22] Y. Li, W. Xiang, Z. Wu, C. Xu, Y. Xu, Y. Xiao, Z. Yang, C. Wu, G. Lv, X. Guo, *Electrochim. Acta* **2018**, *291*, 84–94.
[23] Y. Zhang, Z. Wang, F. Yu, L. Que, M. Wang, Y. Xia, Y. Xue, J. Wu, *J. Power Sources* **2017**, *358*, 1–12.
[24] L. Wu, X. Tang, X. Chen, Z. Rong, W. Dang, Y. Wang, X. Li, L. Huang, Y. Zhang, *J. Power Sources* **2020**, *445*, 227337.
[25] M. Du, P. Yang, W. He, S. Bie, H. Zhao, J. Yin, Z. Zhou, J. Liu, *J. Alloys Compd.* **2019**, *805*, 991–998.
[26] L. Wang, G. Liu, X. Ding, C. Zhan, X. Wang, *ACS Appl. Mater. Interfaces* **2019**,.*11*, 33901–33912.
[27] Y. Levartovsky, X. Wu, C. Erk, S. Maiti, J. Grinblat, M. Talianker, D. Aurbach, *Batteries Supercaps* **2021**, *4*, 221–231.

Manuscript received: March 13, 2023
Revised manuscript received: April 14, 2023
Accepted manuscript online: April 24, 2023
Version of record online: April 27, 2023